Generation of heralded vector-polarized single photons in remotely controlled topological classes

Samuel Corona-Aquino [ORCID],[1] Zeferino Ibarra-Borja [ORCID],[1] Omar Calderón-Losada [ORCID],[2] Bruno Piccirillo [ORCID],[3,4]
Verónica Vicuña-Hernández [ORCID],[3,5] Tonatiuh Moctezuma-Quistian [ORCID],[1] Hector Cruz-Ramírez,[1]
Dorilian Lopez-Mago,[6] and Alfred B. U'Ren[1,*]

[1]*Instituto de Ciencias Nucleares, Universidad Nacional Autónoma de México, Apartado Postal 70-543, 04510 Cd. Mx., Mexico*
[2]*Centro de Investigacion e Innovación en Bioinformatica y Fotonica, Edificio E20 No. 1069, Universidad del Valle, Cali, Valle del Cauca 760042, Colombia*
[3]*Dipartimento di Fisica "Ettore Pancini", Università degli Studi di Napoli Federico II, Napoli 80126, Italy*
[4]*INFN, Sez. di Napoli, Complesso Universitario di Monte Sant'Angelo, via Cinthia, Napoli 80126, Italy*
[5]*CNR-INO, Istituto Nazionale di Ottica, Via Campi Flegrei 34, I-80078 Pozzuoli (NA), Italy*
[6]*Escuela de Ingeniería y Ciencias, Tecnologico de Monterrey, Monterrey N.L. 64849, Mexico*

We demonstrate an experimental protocol for the preparation and control of heralded single photons in inhomogeneously polarized states, such as vector vortex and full Poincaré beam states. A laser beam is shaped by a voltage-controlled spin-to-orbital angular momentum converter q-plate device, which eliminates the need for an interferometer for the robust preparation of high-quality inhomogeneously polarized beams. Such a beam is then used as a pump in a spontaneous parametric down-conversion (SPDC) photon-pair source. We demonstrate the full pump to heralded single-photon transfer of the intensity and phase distributions, as well as of the vector polarization structure. Additionally, we show that by controlling the polarization to which the heralding idler photon is projected before detection, we can toggle between the direct and basis-switched pump-single-photon transfer. We show that this nonlocal control of the heralded single photon pertains also to the topological class of the resulting heralded single photon. We believe that our work will lead to opportunities in photon-based quantum information processing science.

I. INTRODUCTION

Polarization singularities of an optical mode are points on the wave front with an undefined local orientation of the polarization ellipse, surrounded by a region of high phase gradient [1]. Intimately related to phase singularities, polarization singularities are encountered in beams with an inhomogeneous polarization distribution [2,3]; in the paraxial regime, they can be viewed as a superposition of two orthogonally polarized states with a spatially varying phase difference. Specifically, the superposition of two modes with opposite helicity (with topological charges ℓ and $-\ell$), and circularly polarized with opposite handedness results in a vector vortex (VV) mode. The resulting polarization is inhomogeneously distributed, locally linear

except on the optical axis, at which the orientation is undefined, creating a V-point singularity [4]. As a second relevant example, the superposition of a circularly polarized, Gaussian TEM$_{00}$ mode ($\ell = 0$) with a helical mode with circular polarization of the opposite handedness results in a mode well described by the stereographic projection of the Poincaré sphere; the specific projection is determined by the relative phase of the superposition. Such beams are typically known as full Poincaré (FP) beams [5], and the optical field over their transverse wave fronts is mainly elliptical with points of undefined orientation known as C points [4].

In the last two decades, the unique optical properties of polarization singularities—that stem from the structural inseparability of orbital angular momentum (OAM) and spin angular momentum (SAM)—have been exploited for an increasing number of applications in both the classical and quantum domains. In the classical domain, VV beams that obey axial amplitude and phase symmetry are sometimes referred to as cylindrical vector beams [6]. In particular, VV beams with radial polarization have attracted interest because they provide optimal focusing, leading to

---

*alfred.uren@correo.nucleares.unam.mx

a strong and localized longitudinal field component [7,8], which has enabled many applications in imaging, including confocal microscopy, two-photon microscopy, second-harmonic generation microscopy [9], third-harmonic generation microscopy [10], and dark-field imaging [10]. This longitudinal component has been shown to permit stable three-dimensional (3D) trapping of metallic nanoparticles [11], empower laser micromachining, [12,13], implement finer optical lithography, increase packing density for optical storage [14], and enable single molecule spectroscopy [15].

Moving on to FP beams, they have been used to unveil topological properties of light [16,17], particularly for optical Möbius strips and optical skyrmions [18,19]. They have also shown potential for polarimetry, involving the use of the resulting polarization pattern for single-shot measurements [20], and for beam shaping using, e.g., resulting in flattop focusing [21].

In the quantum domain, specifically for photon pairs generated by the spontaneous parametric down-conversion (SPDC) process, vector polarization properties open up avenues for the engineering of correlations and entanglement involving the polarization and OAM degrees of freedom. For example, entangled pairs of VV photons [22] of arbitrary order have been generated using a q plate, a birefringent retardation wave plate with a topologically charged optic-axis distribution that can couple or decouple spin and orbital angular momentum distributions [23]. Hyperentanglement between time-frequency modes and VV modes has been also demonstrated [24], thus enabling protocols such as complete Bell-state analysis [25] and logic gate slimming [26]. While VV beams have been generated both actively [27,28]—i.e., via laser intracavity devices—and passively—through extra-cavity devices [29]—entangled photons in VV modes have so far been generated in a two-step sequence. Thus, single photons are first generated in standard modes, which are subsequently transformed into structured modes using dedicated optical components [22,24,30–32]. However, generating structured single photons directly at the source could prove to be more convenient for compactness, flexibility, and/or scalability in the implementation of quantum information protocols. The polarization and phase structure of VV beams has been transferred from the pump to the signal and idler in stimulated parametric down-conversion [33]. In spontaneous parametric down-conversion (SPDC), however, only the transfer of the scalar vortex structure from the pump to single photons has been already demonstrated [34–36]. In this study, we demonstrate the generation of *vector-polarized* single photons directly from the SPDC process. Our experimental design incorporates a voltage-controlled q plate for the robust and alignment-free preparation of VV or FP beams, which are used to pump a polarization-entangled photon-pair source based on a dual type-I SPDC crystal [37], resulting in the generation of

hybrid-entangled photon pairs. As will be seen, in such a source, projecting the polarization of one of the photons of a given pair before its detection allows nonlocal control of the vector mode of its twin (including its topological class), paving the way for proposing alternative quantum information protocols that exploit this capability.

II. THEORY

A q plate is an electro-optical geometric phase element consisting of a liquid-crystal-based retardation wave plate with a topologically charged axis distribution, capable of converting photon spin angular momentum (SAM) into orbital angular momentum (OAM) and vice versa. The action of a q plate can be described by the operator shown in Eq. (1), where the state $|e, \ell\rangle$ represents an optical mode with polarization $e \in \{L, R\}$ and OAM topological charge $\ell = 2q$ (in a quantum inspired ket notation) [4]. In Eq. (1), ϕ is the spatial azimuthal polar angle and α_0 a constant angle representing a uniform azimuthal shift with respect to the frame of reference. The Pancharatnam-Berry phase $\pm 2(q\phi + \alpha_0)$, imparted to the input photons, when $\delta \neq 2k\pi$, has a helical structure with topological charge $2q$, and is accompanied by a polarization handedness reversal. The retardation δ is electrically controlled using an applied external voltage of a few volts. When $\delta = (2k + 1)\pi$, where k can be any integer number (half-wave operation), the q plate achieves maximum conversion efficiency and the polarization handedness is fully reversed.

$$
\begin{aligned}
\hat{Q}(\delta, q) = \cos\frac{\delta}{2} \left(|L, 0\rangle \langle L, 0| + |R, 0\rangle \langle R, 0| \right) \\
+ i\sin\frac{\delta}{2} \left(e^{i2\alpha_0} e^{i2q\phi} |R, 2q\rangle \langle L, 0| \right. \\
\left. + e^{-i2\alpha_0} e^{-i2q\phi} |L, -2q\rangle \langle R, 0| \right).
\end{aligned}
\tag{1}
$$

When the input polarization state is linear and $\delta = (2k + 1)\pi$, a V point is formed. In contrast, when input polarization is circular and $\delta = (2k + 1)\pi/2$, a C point is formed. Specifically, when $\delta = \pi/2$ and the impinging beam is a TEM_{00} mode in the polarization state $|L\rangle$, the output beam becomes a coherent superposition of a right-circularly polarized beam with geometric phase $\pm(2q\phi + \alpha_0)$ and a left-circularly polarized TEM_{00} mode. If the impinging light has $|R\rangle$ polarization, the output beam becomes a coherent superposition with handedness and geometric phase reversed (compared to the aforementioned case). For $\delta = \pi$, a linearly polarized TEM_{00} mode is turned into a coherent superposition of right- and left-handed polarized beams with opposite topological charge. Thus, by selecting the phase retardation δ and the input polarization state, we can select the superposition, leading to either VV beams or FP beams.

Therefore, our q plate enables the preparation of the pump for the SPDC process in the form

$$|\psi\rangle_{\text{pump}} = \frac{1}{\sqrt{2}} \left(|L, \ell_p\rangle + e^{i\varphi} |R, \ell_p'\rangle \right), \qquad (2)$$

where φ is a fixed phase that can be controlled by a half-wave plate following the q plate. Note that such a state includes VV beams and FP beams as special cases, namely,

$\{\ell_p, \ell_p'\} = \{j, -j\}$ for VV beams and $\{\ell_p, \ell_p'\} = \{j, 0\}$ for FP beams, where $j \in \mathbb{N}$.

In the following section, we discuss our experiments using a type-I dual-crystal SPDC source. In the first (second) crystal the process $H \rightarrow VV$ ($V \rightarrow HH$) occurs, which involves the annihilation of a horizontally (vertically) polarized pump photon and the generation of vertically (horizontally) polarized photon pairs. The resulting SPDC state can be expressed as

$$|\psi\rangle_{\text{SPDC}} = \frac{1}{2} \sum_{\ell_i, \ell_i', \ell_i'', \ell_i'''} \left[c_{\ell_i} |V, \ell_p - \ell_i\rangle_s |V, \ell_i\rangle_i + e^{i\varphi} c_{\ell_i'} |V, \ell_p' - \ell_i'\rangle_s |V, \ell_i'\rangle_i \right.$$
$$\left. - i e^{i\phi} \left(c_{\ell_i''} |H, \ell_p - \ell_i''\rangle_s |H, \ell_i''\rangle_i - e^{i\varphi} c_{\ell_i'''} |H, \ell_p' - \ell_i'''\rangle_s |H, \ell_i'''\rangle_i \right) \right], \qquad (3)$$

where the subscripts refer to the signal (s) and idler (i) photons and ϕ represents a possible phase difference in the contributions to the state from the two crystals. Since we are interested in the preparation of the signal photon state, we project the two degrees of freedom of the idler photon, i.e. OAM and polarization, in a specific way before its detection. First, we project the SPDC two-photon state in such a way that only the vanishing OAM contribution remains for the idler photon. This is achieved experimentally by coupling the idler photon to an optical fiber, resulting in the state

$$|\Psi\rangle = |\ell = 0\rangle_{ii}\langle \ell = 0|\psi\rangle_{\text{SPDC}}$$
$$= \frac{1}{4} \left[\left(|V, \ell_p\rangle_s + e^{i\varphi} |V, \ell_p'\rangle_s \right) |V, 0\rangle_i \right.$$
$$\left. - i e^{i\phi} \left(|H, \ell_p\rangle_s - e^{i\varphi} |H, \ell_p'\rangle_s \right) |H, 0\rangle_i \right]. \qquad (4)$$

Second, we additionally project the former two-photon state onto each of the four idler-photon polarizations $|A\rangle_i$, $|D\rangle_i$, $|L\rangle_i$, and $|R\rangle_i$, resulting in the state $|\Psi\rangle \rightarrow |e\rangle_{ii}\langle e|\Psi\rangle \equiv |u_e\rangle_s |e, 0\rangle_i$, where $|u_e\rangle_s$ represents the conditioned signal-photon state in the following manner:

$$|u_A\rangle_s = \frac{1}{\sqrt{2}} \left(|L, \ell_p\rangle_s + e^{i\varphi'} |R, \ell_p'\rangle_s \right), \qquad (5)$$

$$|u_D\rangle_s = \frac{1}{\sqrt{2}} \left(|R, \ell_p\rangle_s + e^{i\varphi'} |L, \ell_p'\rangle_s \right), \qquad (6)$$

$$|u_L\rangle_s = \frac{1}{\sqrt{2}} \left(|D, \ell_p\rangle_s + e^{i\varphi'} |A, \ell_p'\rangle_s \right), \qquad (7)$$

$$|u_R\rangle_s = \frac{1}{\sqrt{2}} \left(|A, \ell_p\rangle_s + e^{i\varphi'} |D, \ell_p'\rangle_s \right), \qquad (8)$$

where $\varphi' = \varphi + \pi$. Here we have assumed that there is no phase difference between the contributions from the two crystals, i.e., $\phi = 0$. Note from Eqs. (2) and (5) that the vector-conditioned structure of the signal photon resulting from the projection of the idler photon to the state $|A, 0\rangle_i$ is the same as that of the pump except for a π phase shift in φ. As will be seen in both experiments and simulations, this π phase shift results in a rigid rotation of the transverse intensity and position-dependent polarimetry by an angle depending on the characteristic disclination index I_C of the pump polarization structure. Specifically, the latter angle is π/N, where $N = |2(I_C - 1)|$, for $I_C \neq 1$, is the number of radial lines characterizing the polarization topography [38]. Thus, for this particular idler-photon projection, the full amplitude of the pump vector (including transverse intensity, phase, and polarization) is transferred to the signal photon within a rigid rotation depending on I_C.

It is interesting to consider the effects of projecting the idler photon to each of the remaining three states, i.e., $|D, 0\rangle_i$, $|L, 0\rangle_i$, and $|R, 0\rangle_i$. Note that when projecting to the state $|D, 0\rangle_i$, the roles of the polarizations L and R are reversed with respect to the state $|u_A\rangle_s$. Projecting to the state $|L, 0\rangle_i$ has the effect of changing the basis, from $\{L, R\}$ to $\{D, A\}$, with respect to the projection to $|A, 0\rangle_i$. Finally, note that similarly to the transformation observed when changing the projection state from $|A, 0\rangle_i$ to $|D, 0\rangle_i$, when changing the projection state from $|A, 0\rangle_i$ to $|D, 0\rangle_i$, the roles of the D and A polarizations are reversed. Thus, due to the additional richness provided by optical fields exhibiting vector polarization, we are not only able to

transfer the amplitude from the pump to a conditioned single photon (as was done previously in Ref. [34,39]), but we have the additional ability to transform the transferred amplitude according to the change of basis and/or the L/R or D/A permutations described above. This is useful because it leads to an additional degree of control over the heralded single photon; for example, in the FP case, it allows us to obtain an FP heralded single photon in different topological classes (i.e., lemon versus star) simply by changing the idler photon projection for the very same setup; this is in contrast to previous work that requires a different setup for each topological class [40].

III. EXPERIMENT

We have designed an experimental setup, see Fig. 1, in which noncollinear, polarization-entangled SPDC photon pairs are generated in a dual bismuth borate (BiBO) crystal [41], followed by the projection of the idler photon to its zero OAM contribution $\ell = 0$, as well as to each of the four polarizations $|A\rangle_i$, $|D\rangle_i$, $|L\rangle_i$, $|R\rangle_i$ in turn. The detection of the projected idler photon then heralds the signal photon, which is detected in coincidence, in a spatially and polarization-resolved manner [42], relying on a polarimeter followed by an ICCD camera.

The pump for the SPDC process is a narrow-band diode laser (Moglabs ECD004; DL) operating at $\lambda_p = 405$ nm and structured with a voltage-controlled q-plate device. A half-wave plate (HWP$_1$) followed by a polarizing beam splitter (PBS$_1$) optimizes the resulting horizontally polarized laser flux. The combination of a quarter-wave plate (QWP$_1$) followed by one of three q-plate devices characterized by their q values: 1/2, 1, or 3/2, is then used to structure the pump into a high-quality VV beam or FP beam. The type of pump beam produced is determined by (i) the choice of q-plate device, (ii) the orientation angle of QWP$_1$ to obtain either linear or circular incident polarization, and (iii) the voltage applied to the q plate. For example, to generate FP pump beams, we rely on the quarter-wave mode of the q plate, set the birefringence to $\delta = \pi/2$ by applying the correct voltage, and use circular incident polarization. In this manner, the state of the pump photons can be prepared as $|\psi\rangle_{\text{pump}} = \left(|L, 2q\rangle + e^{i\varphi}|R, 0\rangle\right)/\sqrt{2}$ with $q \in \{1/2, 1, 2/3\}$. In contrast, in order to prepare VV pump beams, we rely on the half-wave mode of the q plate by setting the birefringence to $\delta = \pi$ and using linear incident polarization. This allows us to prepare the pump photons in the state $|\psi\rangle_{\text{pump}} = \left(|L, 2q\rangle + e^{i\varphi}|R, -2q\rangle\right)/\sqrt{2}$.

The resulting vector beam is then imaged onto the dual BiBO using a telescope consisting of lenses L_1 ($f_1 = 30$ mm) and L_2 ($f_2 = 40$ mm). Each of the 500-μm-thick BiBO crystals can produce SPDC photon pairs by noncollinear, frequency-degenerate, type-I SPDC; note that the pump coherence length of approximately 30 m is much longer than the combined crystal length, ensuring that the

contributions from the two crystals are coherently added. Note that in our experiment the pump is loosely focused at the crystal with a beam waist radius of $w_0 = 2.2$ mm, leading to a confocal parameter $2\pi w_0^2/\lambda$ of around 70 m, many times longer than the combined crystal length (1 mm). We remark that this implies that our experiment is well within the short-crystal regime in which walkoff effects become negligible. In this regime, note that the single-photon spatial profiles and polarimetries are well inherited from the pump (with some experimental error) as is evident from Figs. 2 and 3. The remaining pump is suppressed by a long-pass filter (transmitting $\lambda > 488$ nm), and the SPDC spectrum is limited by an 800 ± 20 nm bandpass filter. A lens (L_3) placed at a distance of one focal length ($f_3 = 50$ mm) from the crystals provides the Fourier transform of the crystal output Fourier plane FP$_1$. We then split the signal and the idler photons by reflecting the latter from a triangular mirror (TM).

For the part of the experimental setup labeled as "remote preparation," the idler photon imaged on the plane FP$_1$ is reimaged onto the Fourier plane FP$_2$ using a $4f$ telescope with $2.5\times$ demagnification, formed by a planoconvex lens L_4 (with focal length $f_4 = 150$ mm) and a planoconvex lens L_5 (with $f_5 = 60$ mm). Between L_5 and FP$_2$, the polarization of the idler photon is projected using a system (PP) consisting of either: (i) a quarter-wave plate followed by a polarization beams plitter for the $|R\rangle$, $|L\rangle$ projections, or (ii) a half-wave plate followed by a polarization beam splitter for the $|D\rangle$, $|A\rangle$ projections. The tip of a multimode fiber (MMF) is placed on FP$_2$ in such a way that its 2D transverse position can be controlled by a pair of computer-controlled linear motors (25-mm travel range and 0.05-μm minimum step). The MMF, chosen to spatially filter higher modes while maintaining a relatively high coincidence count rate [34,35], is then connected to a fiber-coupled Si avalanche photodiode (APD).

The signal photon on the plane FP$_1$ is transmitted through a quarter-wave plate (QWP$_2$) and a lens L_6 (with $f_6 = 400$ mm), which directs it to the image-preserving delay line (OD) consisting of a polarizing beam splitter (PBS$_3$) and a series of telescopes in the $4f$ configuration, as shown in the lower right panel of Fig. 1. Note that QWP$_2$ and PBS$_3$ form a polarimeter that is used to recover the Stokes parameters of the signal photon. The delay line (OD) is composed of lenses L_7 to L_{11} (with $f_7 = f_8 = f_9 = 750$ mm and $f_{10} = f_{11} = 100$ cm). A quarter-wave plate (QWP$_3$) with its fast axis oriented at $45°$ is used to ensure that upon its return trip (following reflection at M$_3$) the signal photon is deterministically reflected by PBS$_3$, thus exiting the delay line towards the detection stage. Note that the signal photon on plane FP$_1$ is relayed (via L_6 and L_7) onto a plane FP$_{1(1)}$ on M$_3$, which is then relayed (via L_8 and L_9) onto plane FP$_{1(2)}$ on M$_5$, and subsequently (via L_{10} and L_{11}) onto plane FP$_{1(3)}$ on M$_7$. On its return trip, the signal photon is relayed back to FP$_{1(2)}$, then onwards

FIG. 1. Experimental setup used for heralding of single photons with controllable FP or VV polarization patterns. A *q*-plate device is used to prepare the pump in a high-quality vector mode (generation). While the idler photon (remote preparation) is projected to a specific polarization and zero OAM prior to its detection, the signal photon (polarimetry and optical delay) is transmitted through an image-preserving delay line (see bottom right for detail), and is sent to a polarimeter prior to detection by an ICCD camera (detection). Our polarization correlation measurements are presented in the bottom left panel.

back to $FP_{1(1)}$, from which it is relayed (via L_7 and L_{12}, the latter with focal length $f_{12} = 400$ mm). The plane FP_1 is relayed to the plane FP_3, which coincides with the position of the ICCD sensor, by means of the lens L_{12} with focal length $f_{12} = 400$ mm. The total delay provided by OD is 65 ns, which is sufficient to slightly overcompensate for the insertion delay of the ICCD camera.

The detection of the idler photon, projected to its zero OAM contribution and to one of the four polarizations $|H\rangle_i$, $|V\rangle_i$, $|L\rangle_i$, and $|R\rangle_i$, is used to trigger the detection of the signal photon by the ICCD camera after passing through the spatially resolved polarimeter. In such a polarimeter, the transmission is modulated by the orientation angle of QWP_2 according to the following expression:

$$I(\theta) = S_0' = \mathbf{M} \cdot \mathbf{S} =$$
$$= \frac{1}{2}\left(S_0 + S_1 \cos^2 2\theta + S_2 \sin 2\theta \cos 2\theta - S_3 \sin 2\theta\right),$$
$$(9)$$

where $\mathbf{S}$ is the Stokes vector of the analyzed light, S_0' is the intensity after the polarimeter, and $\mathbf{M}$ is the polarimeter response, which is a function of the orientation angle of QWP_2. We rotate QWP_2 in $\pi/8$ radian steps, collecting a total of eight transverse intensity patterns. According to Eq. (9) this system is described by $S_0' = \mathbf{M} \cdot \mathbf{S}$, so that using the pseudoinverse of $\mathbf{M}$ we get $\mathbf{M}^{-1} S_0' = \mathbf{M}^{-1} \cdot \mathbf{S} = \mathbf{S}$, which leaves us with $\mathbf{S}$, from which we can plot the polarization ellipses in the transverse profile of the photon [43].

To ensure that both crystals contribute coherently to the two-photon state, an auxiliary polarization correlation measurement with standard coincidence detection via two avalanche photodiodes in front of the dual crystals was performed [37]. For this purpose, a diagonally polarized Gaussian beam was used to generate the SPDC pair, and with a fixed polarization projection of the idler photon and a variable polarization projection of the signal photon, the polarization correlation was recovered as shown in Fig. 1 (bottom left), from which we obtain visibilities of 98.12%
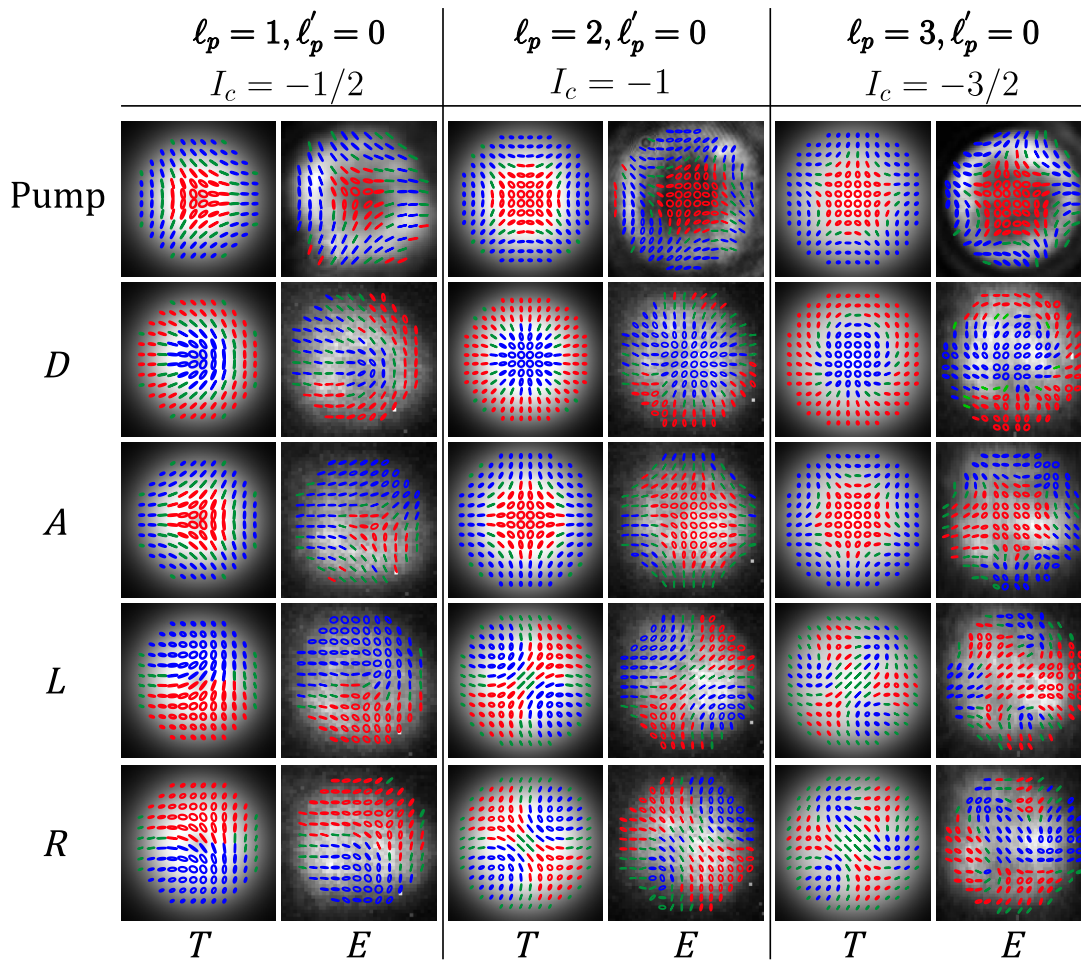
FIG. 2. Vector beam structure for the pump and the heralded signal photon in the case of quarter-wave plate q-plate operation leading to a FP mode profile [the transverse intensity shown in gray scale and the position-dependent polarization in a tricolor map, where green indicates linear polarization and blue (red) indicates left (right) polarization handedness]. While the first row corresponds to the pump, the four remaining rows correspond to the heralded signal photon when the idler is projected to each of the zero-OAM states $|D\rangle$, $|A\rangle$, $|L\rangle$, $|R\rangle$. The columns are organized in pairs, where the left-hand column represents a simulation (T) while the right-hand column represents the corresponding experimental measurement (E).

for the idler projection to H or V and 96.17% for the idler projection to A or D. As is well known, a unit visibility over different bases is consistent with maximal polarization entanglement.

IV. DISCUSSION

The main results of this work are shown in Figs. 2 and 3, for the specific cases of full Poincaré beams and vector vortex beams, respectively. Since we have used three different q-plate devices with q values: 1/2, 1, and 3/2, each of these two figures is organized into three groups of two columns labeled according to the value of q. Within each group, the left-hand column shows a simulation of the transverse intensity and position-dependent polarimetry, while the right-hand column shows the corresponding experimental measurement. In each panel, the transverse

intensity is plotted in gray scale, while the polarization ellipses are plotted on a matrix of points according to a tricolor map, where green represents linear polarization and blue (red) represents left (right) polarization handedness. Note that while the first row corresponds to a measurement of the pump state produced by each of the three q plates, each of the remaining four rows corresponds to the transverse intensity and position-dependent polarimetry for the signal photon as the idler photon is projected into each of the following zero OAM states: $|D, 0\rangle_i$, $|A, 0\rangle_i$, $|R, 0\rangle_i$, or $|L, 0\rangle_i$, as indicated. The pump vector polarization prepared in the case of FP beams (quarter-wave q-plate operation) as well as the VV beams (half-wave q-plate operation) are shown in Table I for each of the three q-plate devices. For the sake of clarity, we have omitted the normalization factor $1/\sqrt{2}$ in this quantum inspired ket notation. Note that we adjust
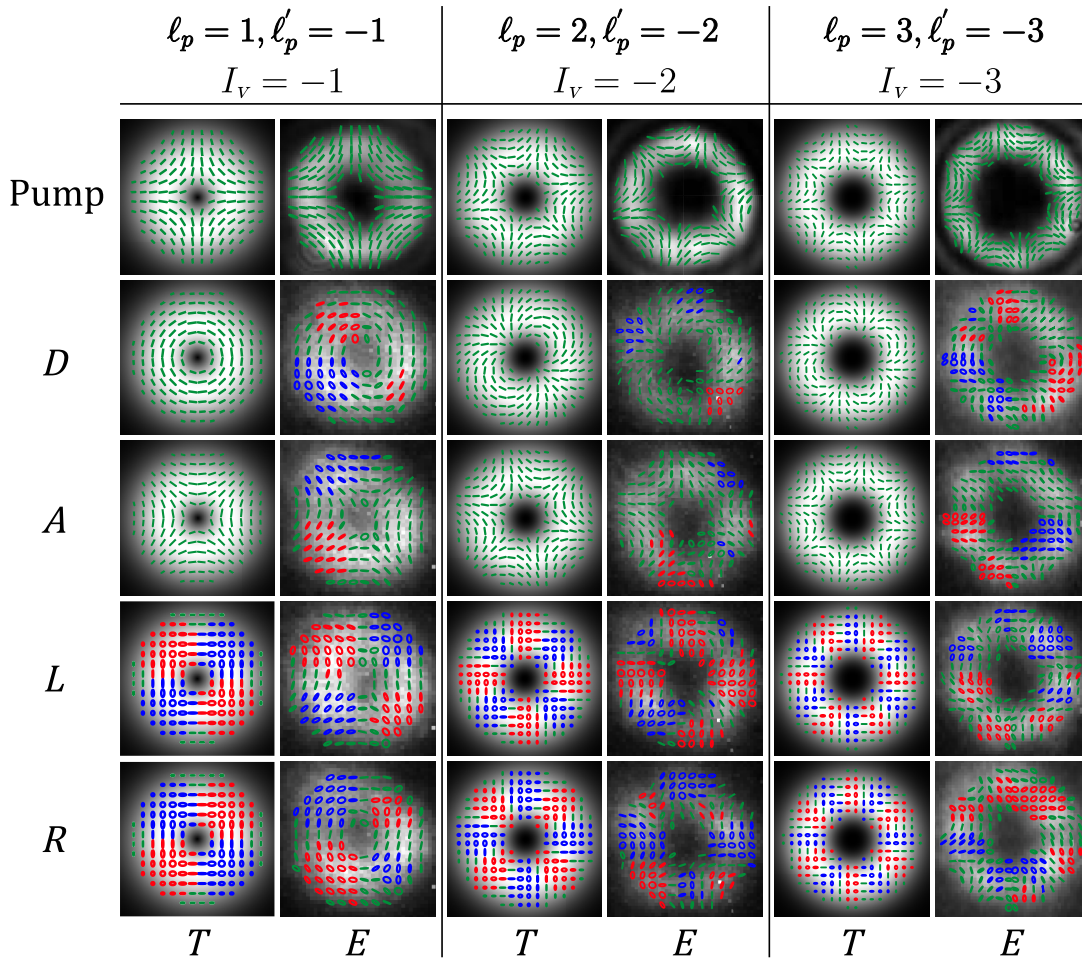
FIG. 3. Vector beam structure for the pump and the heralded signal photon in the case of half-wave plate q-plate operation leading to a VV mode profile [the transverse intensity is shown in gray scale and the position-dependent polarization in a tricolor map, where green indicates linear polarization and blue (red) indicates left (right) polarization handedness]. While the first row corresponds to the pump, the remaining four rows correspond to the signal photon when the idler is projected into each of the zero-OAM states $|D\rangle$, $|A\rangle$, $|L\rangle$, $|R\rangle$. The columns are arranged in pairs, with the left column representing a simulation and the right column representing the corresponding experimental measurement.

the value of φ in the six cases so that the transverse intensity and position-dependent polarimetry matches the azimuthal orientation of the experimental measurement; we thus obtain $\varphi = 0$ for $q = 1/2$, $\varphi = \pi$ for $q = 1$, and $\varphi = \pi/4$ for $q = 3/2$. As expected (see Sec. II above), when we detect the idler photon following its projection to each of the $|D, 0\rangle_i$, $|A, 0\rangle_i$, $|R, 0\rangle_i$, and $|L, 0\rangle_i$ states, the resulting heralded signal photon is characterized by a vector structure, which either corresponds directly to that of the pump (except for a rigid rotation), for projection to $|A, 0\rangle_i$, or is the result of one of three transformations: (i) the roles of the R/L polarizations is permuted, (ii) the basis is changed according to $\{L, R\} \rightarrow \{A, D\}$, or (iii) the basis is changed in addition to then permuting the roles of the A/D polarizations. We thus extend the ability to transfer the transverse intensity and phase from the pump to a heralded single photon from an SPDC

photon pair [34,35,39], to in addition also transferring the full vector polarization structure. Interestingly, by also controlling the polarization to which the idler photon is projected, we are able to exert useful control over the properties of the heralded signal photon. This control includes the possibility of modifying the topological class, in particular, the characteristic disclination index I_C to which the single-photon vector structure belongs; for example, the FP with $q = 1/2$ case produces first-order polarization singularities, with disclination index $I_C = \pm 1/2$, and we can transition from a lemon structure when projecting to $|D, 0\rangle_i$ to a star structure when projecting to $|A, 0\rangle_i$, to a bipolar structure when projecting to $|L, 0\rangle_i$ or $|R, 0\rangle_i$. This topological class transition also occurs for the higher-order disclinations with $I_C = \pm 3/2$, produced when $q = 3/2$, and transitioning from a hyperlemon structure when projecting to $|D, 0\rangle_i$ to a hyperstar structure when projecting

TABLE I. Resulting vector polarized pump for each q-plate device in quarter-wave operation to prepare FP beams and in half-wave operation to prepare VV beams. We have omitted the normalization factor $1/\sqrt{2}$ for the sake of clarity while the φ value is displayed in the main text.

	Prepared pump	
q	FP beams	VV beams
1/2	$\left(|L,1\rangle + e^{i\varphi}|R,0\rangle\right)$	$\left(|L,1\rangle + e^{i\varphi}|R,-1\rangle\right)$
1	$\left(|L,2\rangle + e^{i\varphi}|R,0\rangle\right)$	$\left(|L,2\rangle + e^{i\varphi}|R,-2\rangle\right)$
3/2	$\left(|L,3\rangle + e^{i\varphi}|R,0\rangle\right)$	$\left(|L,3\rangle + e^{i\varphi}|R,-3\rangle\right)$

to $|A,0\rangle_i$, to a hexapolar structure when projecting to $|L,0\rangle_i$ or $|R,0\rangle_i$. The structures produced by $q=1$ transition from a radial FP beam when projecting to $|D,0\rangle_i$ to a hyperstar structure with $I_C = -1$ when projecting to $|A,0\rangle_i$), to a quadrupolar structure when projecting to $|L,0\rangle_i$ or $|R,0\rangle_i$. Thus, beyond pump-single heralded photon amplitude transfer, we are able by projecting and detecting the idler photon to, nonlocally, determine the vector polarization structure of the signal photon, which in some cases presents slight variations from the expected pattern. These discrepancies, e.g., the appearance of elliptical or circular polarization components in cases where linear polarization is expected (see projections A and D in Fig. 3) could be due to a misalignment introduced by the QWP rotation in the context of a slight nonconcentricity of the two overlapped modes that make up the VV or FP modes at the single-photon level; such imperfections can be significant considering that the LG mode diameter is in the order of hundreds of microns. In Fig. 4, we show a simulation of the transverse intensity and of the polarization distribution resulting from making the two constituent modes slightly nonconcentric, in comparison to the ideal case. Note that while the pair of modes being superposed is identical in both scenarios, the effect of the lateral relative shift of the constituent modes on the polarization distribution clearly resembles the behavior observed in our experimental measurements. This effect could apply to the two pump constituent modes (to be "inherited" by the signal and idler photon pair) or could apply to the two coherently added contributions to the two-photon state from the two SPDC crystals in our source.

As has been pointed out, the correct pump-single-heralded-photon full-vector-amplitude transfer requires the use of a dual crystal so that both the horizontally and vertically polarized components are individually transferred. Let us briefly consider examples of experimental measurements in which the effect of one of the two crystals is nullified, obtained by projecting the idler photon to either $|H,0\rangle_i$ or $|V,0\rangle_i$. In Fig. 5, we present measurements similar to those in the previous two figures, obtained for a FP pump beam with $q=1/2$ (first and second columns), and for a VV pump beam with $q=1$ (third and fourth
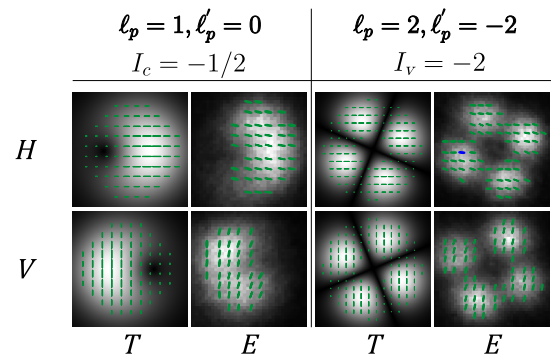

FIG. 4. This figure illustrates the effect of imperfect overlap between the two constituent LP modes of an FP mode. In the upper row we show the ideal case involving two concentric modes giving rise to an ideal FP beam (third column). The bottom row shows the effect of a slight nonconcentricty between the two constituent LP modes, leading to a noticeable polarization distribution deformation. The colormap is as the shown in Figs. 2 and 3.

columns). In this figure, while the first row corresponds to projecting on $|H,0\rangle_i$ the second row corresponds to projecting on $|V,0\rangle_i$. The key point to notice is that in all of these measurements, the measured polarization pattern is homogeneous, i.e., the vector polarization structure is suppressed. Furthermore, it may be seen that there is no indication of pump-single-heralded-photon transfer, as there was in the two previous figures.
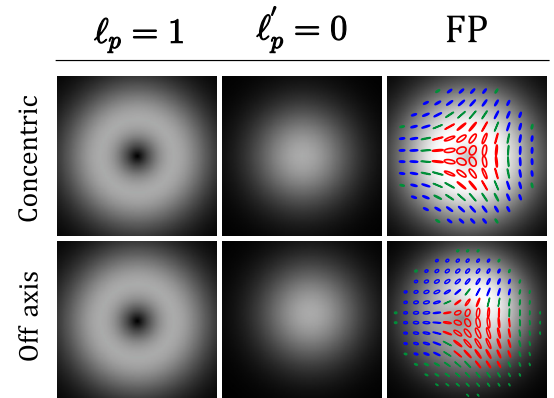

FIG. 5. The effect of projecting to the state $|H,0\rangle$ (first row) or $|V,0\rangle$ (second row) is shown, for comparison to Fig. 2 (case $q=1/2$) and to Fig. 3 (case $q=1$). The columns are organized in two groups; while the first column corresponds to a $q=1/2$ q plate in which the pump was prepared in the state $\left(|L,1\rangle + e^{i\varphi}|R,0\rangle\right)/\sqrt{2}$, the second one corresponds to $q=1$ q plate with a pump state given by $\left(|L,2q\rangle + e^{i\varphi}|R,-2q\rangle\right)/\sqrt{2}$. Within each group: the left column shows a simulation (T) and the right column shows the corresponding experimental measurement (E). As can be seen, all the polarization ellipses are in fact linear according to the tricolor map stated in Figs. 2 and 3.

V. CONCLUSIONS

In this paper, we have demonstrated an experimental protocol for the heralding of single photons described by a controllable vector polarization structure. Our work relies on the use of voltage-controlled q-plate devices, for the robust preparation of vector vortex (VV) and full Poincaré (FP) beams. We remark that our q-plate approach eliminates the need for a free-space interferometer, thus yielding a simplified and more stable experimental setup. Such high-quality vector beams are then used as pump in a spontaneous parametric down-conversion (SPDC) photon-pair source. We have demonstrated the transfer of the full amplitude of a vector beam (including intensity, phase, and vector polarization) to a single photon, heralded from the SPDC photon pair by projection and detection of its idler twin. Furthermore, we have shown that we can control, nonlocally, the resulting signal-photon vector amplitude by selecting the particular projection of the idler photon, to one of the following zero-OAM states $|A,0\rangle_i$, $|D,0\rangle_i$, $|L,0\rangle_i$, and $|R,0\rangle_i$. This control enables us, on the one hand, to obtain the heralded single photon described by a pump-transferred amplitude in the $\{L,R\}$ or $\{A,D\}$ bases, or in versions of these with permuted roles for R/L and A/D, and on the other hand it allows us to, again nonlocally, to modify at will the topological class of the resulting heralded vector structure. We expect that this type of control over the vector structure of single photons will open up exciting possibilities for quantum communications and information processing.

[1] Ruchi, P. Senthilkumaran, and S. K. Pal, Phase singularities to polarization singularities, Int. J. Opt. **2020,** 2812803 (2020), publisher: Hindawi.

[2] H. R.-D. *et al.*, Roadmap on structured light, J. Opt. **19,** 013001 (2016).

[3] Y. Shen, Q. Zhang, P. Shi, L. Du, X. Yuan, and A. V. Zayats, Optical skyrmions and other topological quasiparticles of light, Nat. Photonics **18,** 15 (2024).

[4] P. Darvehi, V. Vicuña-Hernández, L. Marrucci, E. Piedipalumbo, E. Santamato, and B. Piccirillo, Increasing the topological diversity of light with modulated Poincaré beams, J. Opt. **23,** 054002 (2021).

[5] A. M. Beckley, T. G. Brown, and M. A. Alonso, Full Poincaré beams, Opt. Express **18,** 10777 (2010).

[6] Q. Zhan, Cylindrical vector beams: From mathematical concepts to applications, Adv. Opt. Photon. **1,** 1 (2009).

[7] K. S. Youngworth and T. G. Brown, Focusing of high numerical aperture cylindrical-vector beams, Opt. Express **7,** 77 (2000).

[8] R. Dorn, S. Quabis, and G. Leuchs, Sharper focus for a radially polarized light beam, Phys. Rev. Lett. **91,** 233901 (2003).

[9] D. P. Biss and T. G. Brown, Polarization-vortex-driven second-harmonic generation, Opt. Lett. **28,** 923 (2003).

[10] S. Carrasco, B. E. A. Saleh, M. C. Teich, and J. T. Fourkas, Second- and third-harmonic generation with vector Gaussian beams, J. Opt. Soc. Am. B **23,** 2134 (2006).

[11] Q. Zhan, Trapping metallic Rayleigh particles with radial polarization, Opt. Express **12,** 3377 (2004).

[12] V. G. Niziev and A. V. Nesterov, Influence of beam polarization on laser cutting efficiency, J. Phys. D: Appl. Phys. **32,** 1455 (1999).

[13] M. Meier, V. Romano, and T. Feurer, Material processing with pulsed radially and azimuthally polarized laser radiation, Appl. Phys. A **86,** 329 (2007).

[14] C. J. R. Sheppard and A. Choudhury, Annular pupils, radial polarization, and superresolution, Appl. Opt. **43,** 4322 (2004).

[15] L. Novotny, M. R. Beversluis, K. S. Youngworth, and T. G. Brown, Longitudinal field modes probed by single molecules, Phys. Rev. Lett. **86,** 5251 (2001).

[16] C. Rosales-Guzmán, B. Ndagano, and A. Forbes, A review of complex vector light fields and their applications, J. Opt. **20,** 123001 (2018).

[17] A. Forbes, M. de Oliveira, and M. R. Dennis, Structured light, Nat. Photon **15,** 253 (2021).

[18] T. Bauer, P. Banzer, E. Karimi, S. Orlov, A. Rubano, L. Marrucci, E. Santamato, R. W. Boyd, and G. Leuchs, Observation of optical polarization Mobius strips, Science **347,** 964 (2015).

[19] R. Gutiérrez-Cuevas and E. Pisanty, Optical polarization skyrmionic fields in free space, J. Opt. **23,** 024004 (2021).

[20] J. C. Suárez-Bermejo, J. C. González de Sande, M. Santarsiero, and G. Piquero, Mueller matrix polarimetry using full Poincaré beams, Opt. Lasers Eng. **122,** 134 (2019).

[21] W. Han, W. Cheng, and Q. Zhan, Flattop focusing with full Poincaré beams under low numerical aperture illumination., Opt. Lett. **36,** 1605 (2011).

[22] V. D'Ambrosio, G. Carvacho, F. Graffitti, C. Vitelli, B. Piccirillo, L. Marrucci, and F. Sciarrino, Entangled vector vortex beams, Phys. Rev. A **94,** 030304 (2016).

[23] B. Piccirillo, S. Slussarenko, L. Marrucci, and E. Santamato, The orbital angular momentum of light: Genesis

and evolution of the concept and of the associated photonic technology, La Rivista del Nuovo Cimento **36**, 501 (2013).

[24] F. Graffitti, V. D'Ambrosio, M. Proietti, J. Ho, B. Piccirillo, C. de Lisio, L. Marrucci, and A. Fedrizzi, Hyperentanglement in structured quantum light, Phys. Rev. Res. **2**, 043350 (2020).

[25] S. P. Walborn, S. Pádua, and C. H. Monken, Hyperentanglement-assisted Bell-state analysis, Phys. Rev. A **68**, 042313 (2003).

[26] B. P. Lanyon, M. Barbieri, M. P. Almeida, T. Jennewein, T. C. Ralph, K. J. Resch, G. J. Pryde, J. L. O'Brien, A. Gilchrist, and A. G. White, Simplifying quantum logic using higher-dimensional Hilbert spaces, Nat. Phys. **5**, 134 (2009).

[27] D. Pohl, Operation of a Ruby laser in the purely transverse electric mode TE01, Appl. Phys. Lett. **20**, 266 (2003).

[28] D. Naidoo, F. S. Roux, A. Dudley, I. Litvin, B. Piccirillo, L. Marrucci, and A. Forbes, Controlled generation of higher-order Poincaré sphere beams from a laser, Nat. Photonics **10**, 327 (2016).

[29] A. Rubano, F. Cardano, B. Piccirillo, and L. Marrucci, Q-plate technology: A progress review [invited], J. Opt. Soc. Am. B **36**, D70 (2019).

[30] R. Fickler, R. Lapkiewicz, S. Ramelow, and A. Zeilinger, Quantum entanglement of complex photon polarization patterns in vector beams, Phys. Rev. A **89**, 060301 (2014).

[31] E. Karimi, J. Leach, S. Slussarenko, B. Piccirillo, L. Marrucci, L. Chen, W. She, S. Franke-Arnold, M. J. Padgett, and E. Santamato, Spin-orbit hybrid entanglement of photons and quantum contextuality, Phys. Rev. A **82**, 022115 (2010).

[32] A. Suprano, D. Zia, M. Pont, T. Giordani, G. Rodari, M. Valeri, B. Piccirillo, G. Carvacho, N. Spagnolo, P. Senellart, L. Marrucci, and F. Sciarrino, Orbital angular momentum based intra- and interparticle entangled states generated via a quantum dot source, Adv. Photonics **5**, 046008 (2023).

[33] N. Rubiano da Silva, A. de Oliveira, M. Arruda, R. Medeiros de Araújo, W. Soares, S. Walborn, R. Gomes, and P. Souto Ribeiro, Stimulated parametric down-conversion with vector vortex beams, Phys. Rev. Appl. **15**, 024039 (2021).

[34] V. Vicuña Hernández, J. T. Santiago, Y. Jerónimo-Moreno, R. Ramírez-Alarcón, H. Cruz-Ramírez, A. B. U'Ren, and R. Jáuregui-Renaud, Double transverse wave-vector correlations in photon pairs generated by spontaneous parametric down-conversion pumped by Bessel-Gauss beams, Phys. Rev. A **94**, 063863 (2016).

[35] M. V. Jabir, N. Apurv Chaitanya, M. Mathew, and G. K. Samanta, Direct transfer of classical non-separable states into hybrid entangled two photon states, Sci Rep **7**, 7331 (2017).

[36] N. Bornman, W. Tavares Buono, M. Lovemore, and A. Forbes, Optimal pump shaping for entanglement control in any countable basis, Adv. Quantum Technol. **4**, 2100066 (2021).

[37] P. G. Kwiat, E. Waks, A. G. White, I. Appelbaum, and P. H. Eberhard, Ultrabright source of polarization-entangled photons, Phys. Rev. A **60**, R773 (1999).

[38] V. Vicuña-Hernández, F. Cardano, P. Darvehi, L. Marrucci, A. Rubano, and B. Piccirillo, Spatial mode analysis of optical beams carrying monstar disclinations, J. Opt. **25**, 044001 (2023).

[39] A. Z. Khoury, P. H. Souto Ribeiro, and K. Dechoum, Transfer of angular spectrum in parametric down-conversion with structured light, Phys. Rev. A **102**, 033708 (2020).

[40] B. Khajavi and E. J. Galvez, High-order disclinations in space-variant polarization, J. Opt. **18**, 084003 (2016).

[41] R. Rangarajan, M. Goggin, and P. Kwiat, Optimizing type-I polarization-entangled photons, Opt. Express **17**, 18920 (2009).

[42] R. S. Aspden, D. S. Tasca, R. W. Boyd, and M. J. Padgett, EPR-based ghost imaging using a single-photon-sensitive camera, New J. Phys. **15**, 073032 (2013).

[43] R. A. Chipman, W. T. Lam, and G. Young, *Polarized Light and Optical Systems* (CRC Press, Boca Raton, Florida, 2018).